

## Chapter 2

# Models and Theory of Polymer Rheology

### 2.1 Introduction

The use of synthetic polymeric materials is ubiquitous in the modern world and so the understanding of their physical properties is important throughout industry [Ber91]. Polymers are not only important in industry; they are also very common in biological systems [Hua05] and beside the practical need for an understanding of their properties, the complexity of these materials pose many interesting and challenging problems for scientists to solve.

In this thesis we will focus on just two significant areas of polymer rheology: microscopic rheological models and molecular dynamics computer simulation of chain molecules.

In this chapter we will introduce and review the rheological theory of polymer fluids. Historically there have been two different approaches to this problem, empirical and theoretical. The focus of this thesis and chapter will be the theoretical models, however some mention will be made of the empirical models. We will concentrate in particular on analytic models of polymer

rheology which are either based on statistical mechanics or microscopically based models.

One of the original aims of this work was to explore methods of comparing results of nonequilibrium molecular dynamics simulations (NEMD) and microscopic models of polymer rheology. Approaching this aim we found that we would have to perform a significant study of the self-diffusion of polymers in fluids out of equilibrium. Consequently a large part of the project has involved analysis of the diffusion properties of these systems under shear and extensional flow. This type of analysis had not been performed in such detail before, and extremely little had been analysed for molecules in extensional flow.

The structure of this chapter is as follows. We begin by introducing the very general field of rheology, and explain the need for constitutive equations. With this motivation we give a brief overview of the constitutive equations found in the literature. We want to focus our attention on the rheology of polymeric liquids, and so this chapter continues with an introduction to some of the chemical and structural properties of polymers. Finally, we can introduce the Rouse and Doi-Edwards models and detail some predictions of these models. We also detail the parameters of the models which need to be measured so that comparisons between simulation and models can be performed.

## **2.2 Continuum mechanics and constitutive equations**

When studying the processing of polymeric liquids it is often necessary to know the macroscopic properties of the liquid's flow. Prediction of the velocity, stress and temperature fields are often sought [Spu97, Ari62] and can be found by solving the equations of motion together with boundary conditions.

The methods of solution for these equations can be analytic [Spu97, Bat67] however for engineering applications there is now an arsenal of numerical methods [Wes01, OP02] and commercial software – such as Fluent or ANSYS CFX.

In this section we introduce the conservation equations for fluids and show the need for constitutive equations. Detailed derivations of these equations are given in many texts, and we note in particular de Groot and Mazur [dGM84].

### Conservation equations

The first of the conservation equations is the equation for conservation of mass

$$\frac{\partial \rho}{\partial t} + \nabla \cdot \mathbf{j} = 0 \quad (2.1)$$

Here  $\mathbf{j}(\mathbf{r}, t)$  is the flux vector. We identify this with the streaming flux  $\mathbf{j}(\mathbf{r}, t) = \rho(\mathbf{r}, t)\mathbf{u}(\mathbf{r}, t)$  where  $\rho = \rho(\mathbf{r}, t)$  is the density of the fluid at position  $\mathbf{r}$  and time  $t$  and  $\mathbf{u} = \mathbf{u}(\mathbf{r}, t)$  is the velocity field of the fluid. We thus obtain the equation,

$$\frac{\partial \rho}{\partial t} + \nabla \cdot (\rho \mathbf{u}) = 0. \quad (2.2)$$

The second conservation equation is for the conservation of momentum, this is,

$$\rho \frac{D\mathbf{u}}{Dt} = \rho \mathbf{f} - \nabla \cdot \mathbf{P}. \quad (2.3)$$

Here  $\mathbf{f}(\mathbf{r}, t)$  is the body force per unit density exerted on the fluid by external fields, for example gravitational or electric.  $\mathbf{P}(\mathbf{r}, t)$  is the pressure tensor in the fluid which corresponds to the force per unit area in the fluid, exerted by the fluid surrounding the position  $\mathbf{r}$  at time  $t$ . The pressure tensor is a  $3 \times 3$  second rank tensor. Considering a small cubic volume of fluid aligned with Cartesian axes, the elements of the pressure tensor are given by  $P_{ij}$  where the notation corresponds to the force per unit area exerted *on* the  $\hat{\mathbf{n}}_j$

directed face in the  $\hat{\mathbf{n}}_i$  direction, where  $i$  and  $j$  are pronumerals for the set of coordinates  $\{x, y, z\}$ . In this thesis we denote tensors either with a Latin pronumeral with a San-serif font or with a Greek pronumeral in a bold font. Vectors have a bold font and scalars a plain font.

The derivative  $\frac{D}{Dt} = \frac{\partial}{\partial t} + \mathbf{u} \cdot \nabla$  is known as the material derivative and corresponds to the rate of change of a field at a fixed *material point* which by definition follows the stream lines. To explain this further, consider making observations of a scalar field  $a(\mathbf{r}, t)$  along an arbitrary path  $\mathbf{q}(t) = (q_x(t), q_y(t), q_z(t))$ . The rate of change of  $a(\mathbf{q}(t), t)$  with respect to time as observed along  $\mathbf{q}(t)$  will be

$$\begin{aligned} \left. \frac{da}{dt} \right|_{\mathbf{q}(t)} &= \frac{\partial a}{\partial t} + \frac{dq_x}{dt} \frac{\partial a}{\partial x} + \frac{dq_y}{dt} \frac{\partial a}{\partial y} + \frac{dq_z}{dt} \frac{\partial a}{\partial z} \\ &= \frac{\partial a}{\partial t} + \dot{\mathbf{q}} \cdot \nabla a. \end{aligned}$$

If instead of following an arbitrary path  $\mathbf{q}(t)$ , we follow the streamlines, then  $\dot{\mathbf{q}}(t) = \mathbf{u}(\mathbf{q}(t), t)$  so that

$$\left. \frac{da}{dt} \right|_{\text{streamline}} \equiv \frac{Da}{Dt} = \frac{\partial a}{\partial t} + \mathbf{u} \cdot \nabla a. \quad (2.4)$$

Thus far we can see that (2.1) and (2.3) correspond to the conservation equations of classical mechanics. We have two more conservation equations to include: firstly the principle of conservation of angular momentum which implies [Gal02] that the pressure should be symmetric:

$$\mathbf{P} = \mathbf{P}^T; \quad (2.5)$$

secondly we have the equation for conservation of energy

$$\rho \frac{De}{Dt} = -\mathbf{P} : \nabla \mathbf{u} - \nabla \cdot \mathbf{j}_Q \quad (2.6)$$

where for arbitrary tensors  $\mathbf{G}$  and  $\mathbf{H}$  with components  $G_{ij}$  and  $H_{ij}$ ,  $\mathbf{G} : \mathbf{H} \equiv \sum_j \sum_i G_{ji} H_{ij} = \text{trace}(\mathbf{G} \cdot \mathbf{H})$  *i.e.* the trace of the matrix product of  $\mathbf{G}$  and  $\mathbf{H}$ . The scalar field  $e(\mathbf{r}, t)$  is the energy density of the system and  $\mathbf{j}_Q$  is the heat flux vector. The velocity gradient  $\nabla \mathbf{u}$  is a tensor given in Cartesian coordinates by,

$$\nabla \mathbf{u} = \begin{pmatrix} \frac{\partial u_x}{\partial x} & \frac{\partial u_y}{\partial x} & \frac{\partial u_z}{\partial x} \\ \frac{\partial u_x}{\partial y} & \frac{\partial u_y}{\partial y} & \frac{\partial u_z}{\partial y} \\ \frac{\partial u_x}{\partial z} & \frac{\partial u_y}{\partial z} & \frac{\partial u_z}{\partial z} \end{pmatrix}. \quad (2.7)$$

Equation (2.6) is an expression of the second law of thermodynamics; the first term on the right hand side of (2.6) is due to work done on a volume element of fluid around  $\mathbf{r}$  at time  $t$ , the second term is due to heat leaving the same element.

### Constitutive equations

The equations we have summarised so far (2.1),(2.3),(2.5) and (2.6) are very general continuum expressions of the conservation laws of mechanics and are valid for all materials. However these equations are not closed, *i.e.* there are more unknowns than equations of motion. Constitutive equations are introduced to overcome this problem.

As an initial example of a constitutive equation (though we do not use it specifically in the remainder of the thesis) we introduce Fourier's law of heat conduction [Fou78, CJ86] which relates the gradient of the temperature to the heat flux vector,

$$\mathbf{j}_Q = -k_T \nabla T(\mathbf{r}, t). \quad (2.8)$$

Here  $k_T$  is the coefficient of thermal conductivity. Considering for simplicity a static system of constant density such that  $\nabla \cdot \mathbf{u} = 0$  we can now obtain the heat equation. We note from thermodynamics that  $\rho \frac{\partial e}{\partial T}|_v = c_v$  with  $c_v$  the heat capacity at constant volume, substitution of this and (2.8) into (2.6)

leads to the heat equation

$$\frac{\partial T(\mathbf{r}, t)}{\partial t} = \frac{k_T}{c_v} \nabla^2 T(\mathbf{r}, t). \quad (2.9)$$

This is a closed linear equation which can be solved using well established techniques [CJ86]. This example illustrates two key points about constitutive relations: firstly the form of the constitutive equation needs to be decided and secondly any coefficients of the models need to be either measured experimentally [RPP87] or calculated using methods which are derived from the physics of the material at an atomic or molecular level [Eva82]. The coefficient of thermal conductivity  $k_T$  is a transport coefficient. A large part of this thesis is devoted to the calculation of several transport coefficients. We also note at this point that the diffusion equation which we focus on in Chapter 5 has the same form as the heat equation.

The preceding derivation illustrates that under flow free conditions the equation for conservation of energy can be closed using Fourier's law for heat conduction (2.8) to give a closed partial differential equation which can then be solved. We now consider the situation for (2.3) the equation for conservation of momentum. To close this equation a relationship between the pressure tensor  $\mathbf{P}$  and the velocity gradient  $\nabla \mathbf{u}$  is required. For simple fluids the following constitutive equation is often used,

$$\mathbf{P} = (p - \eta_V \nabla \cdot \mathbf{u}) \mathbf{I} - \eta \left( \nabla \mathbf{u} + (\nabla \mathbf{u})^T \right). \quad (2.10)$$

Here  $p \equiv \frac{1}{3} \text{trace}(\mathbf{P})$  is the isotropic pressure,  $\eta_V$  is the bulk viscosity,  $\mathbf{I} = \text{diag}(1, 1, 1)$  is the unit tensor and  $\eta$  is the shear viscosity and is independent of the flow. The symmetric tensor in the last term is known as the strain-rate tensor

$$\dot{\boldsymbol{\gamma}}(\mathbf{r}, t) = \nabla \mathbf{u}(\mathbf{r}, t) + (\nabla \mathbf{u}(\mathbf{r}, t))^T. \quad (2.11)$$

By isolating the hydrostatic pressure  $p$ , (2.10) also leads to a definition of the stress tensor  $\boldsymbol{\sigma}$ :

$$\mathbf{P} = p\mathbf{I} - \boldsymbol{\sigma}. \quad (2.12)$$

The stress tensor has the same rank and dimension as the pressure tensor, however it has the opposite sign.

At this point the coefficients  $\eta_V$  and  $\eta$  are constants, independent of the strain-rate. Fluids for which the pressure tensor obeys (2.10) are known as “Newtonian fluids” – see Newton’s *Principia* [New99], first published in 1687. Combining (2.10) with (2.3) leads to the Navier-Stokes equations which have been analysed in great detail [Gal02]. For the case of an incompressible fluid with a known external force  $\mathbf{f}(\mathbf{r}, t)$  the Navier-Stokes equations are [Ari62],

$$\frac{\partial \mathbf{u}}{\partial t} + \mathbf{u} \cdot \nabla \mathbf{u} = \mathbf{f} - \nabla p + \eta \nabla^2 \mathbf{u} \quad (2.13)$$

$$\nabla \cdot \mathbf{u} = 0. \quad (2.14)$$

There are now an equal number of equations and unknowns. However, unlike the heat equation (2.9) which is linear in  $T(\mathbf{r}, t)$ , (2.13) is nonlinear in  $\mathbf{u}(\mathbf{r}, t)$  due to the term  $\mathbf{u} \cdot \nabla \mathbf{u}$ . We can use separation of variables to isolate and solve for the pressure in terms of the external force. In the case of a conservative force with a potential  $\phi(\mathbf{r})$  a new pressure can be defined  $\mathbf{p}' = \mathbf{p} + \phi$  so that the force and pressure term in (2.13) combine. Further analysis of the Navier-Stokes equations is beyond the scope of this thesis, however, introductory and advanced material can be found in a wealth of textbooks including [Bat67, Fri95].

As for the thermal conductivity in (2.8) and (2.9) the viscosities  $\eta$  and  $\eta_V$  are transport coefficients which need to be determined either by direct experiment or from statistical mechanical models relying again on atomic or molecular properties of the fluid. In Chapter 3 we introduce the molecular dynamics techniques which can be used to do these calculations, while the

remainder of this chapter is devoted to constitutive equations for polymeric liquids, several of which are based on kinetic or stochastic models of the fluid.

### 2.3 Rheology and phenomenological constitutive equations

In the last section we explained the need for constitutive equations and in particular we introduced the Newtonian constitutive equation (2.10) which related the pressure tensor in a fluid to the strain-rate tensor. Though (2.10) is accurate for simple liquids and is obeyed by many liquids at low strain rates, for complex liquids the constitutive equation can be a more involved relation often dependent on the flow history of the liquid.

The study of constitutive equations for flow comes under the topic of Rheology. The definition of rheology was refined at an early meeting of the society of Rheology (1929) to be “the study of flow and deformation of all forms of matter” [Rei64]. The topic includes the experimental investigation of these properties. To carefully characterise fluids experiments are performed for which the strain rate profile in the liquid is known. The types of flow studied by rheologists include: steady state homogeneous flow which we explain in more detail below; the start up of flow; stress relaxation after the cessation of flow.

#### Homogeneous Flows

In rheological experiments the type of flow observed is carefully controlled so that clear experimental results are obtained (see for example Bird *et al.* [BAH87] Chapter 10). In particular homogeneous flows are common. In a homogeneous flow the velocity gradient is independent of position and time. In this thesis we look at planar Couette flow (PCF) and planar extensional

flow (PEF). The velocity gradient tensor for these flows is,

$$\nabla \mathbf{u} = \begin{pmatrix} +\dot{\epsilon} & 0 & 0 \\ \dot{\gamma} & -\dot{\epsilon} & 0 \\ 0 & 0 & 0 \end{pmatrix} \quad (2.15)$$

With  $\dot{\epsilon} = 0$  for PCF and  $\dot{\gamma} = 0$  for PEF. A whole range of steady flows are possible, and one can parameterise the extensional flows with the velocity gradient tensor,

$$\nabla \mathbf{u} = \text{diag}(+\dot{\epsilon}, -\dot{\epsilon}(1+m), +\dot{\epsilon}m), \quad (2.16)$$

where  $-\frac{1}{2} \leq m \leq +1$ , with  $\dot{\epsilon} > 0$ , for uniaxial extensional flow  $m = -\frac{1}{2}$ , while for biaxial flow  $m = +1$ . For planar extensional flow  $m = 0$ . Note that for comparison with [Dea95], we have swapped the second and third element in  $\nabla \mathbf{u}$ , to conform with past simulation works of colleagues.

Diagrams of these flows are shown in Fig. 2.1. The streamlines for PEF are hyperbolic with an unstable fixed point at the origin. In the geometry we have chosen for PCF the streamlines are parallel with the  $x$ -axis and there is a velocity gradient  $\dot{\gamma}$  in the  $y$  direction. One can also consider mixed flows which combine both shear and extension. In the body of this thesis we just consider PCF and PEF (however, see appendix 1 for a discussion of suitable periodic boundary conditions for NEMD simulations of planar mixed flows).

In discussing these homogeneous flows it helps to consider the finite strain. We consider the deformation gradient tensor  $\mathbf{E}(t, t')$  which transforms a material point at  $t'$  to its corresponding point at  $t$ , as follows,

$$\mathbf{r}(t) \rightarrow \mathbf{r}(t') = \mathbf{E}(t, t') \cdot \mathbf{r}(t') \quad (2.17)$$

where  $\mathbf{r}(t')$  is an arbitrary material point. For planar Couette and planar

extensional flow  $\mathbf{E}(t, t')$  can be found from the velocity gradient to be,

$$\mathbf{E}(t, t') = \begin{pmatrix} \exp[\dot{\epsilon}(t-t')] & \dot{\gamma}(t-t') & 0 \\ 0 & \exp[-\dot{\epsilon}(t-t')] & 0 \\ 0 & 0 & 1 \end{pmatrix} \quad (2.18)$$

For planar Couette flow  $\dot{\epsilon} = 0$  and for planar extensional flow  $\dot{\gamma} = 0$ . The strain here is a linear function of the position; in contrast for an inhomogeneous flow the strain will be nonlinear.

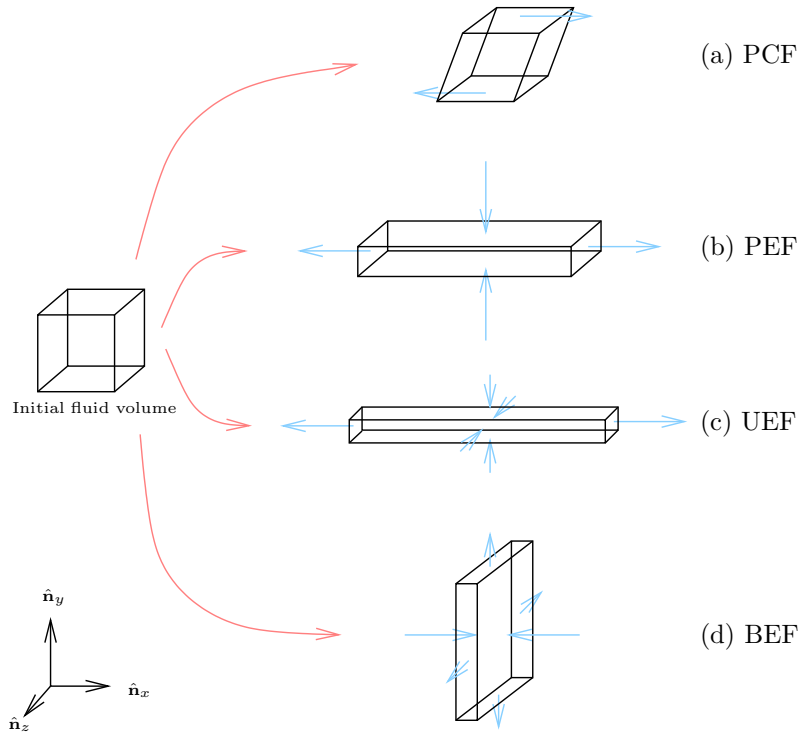


Figure 2.1: An initial fluid volume undergoes a specific deformation in each of these examples of an homogeneous flow: (a) For planar Couette flow (PCF) the volume is sheared; (b) For planar extensional flow (PEF) there is compression parallel to the  $y$ -axis and extension parallel to the  $x$ -axis; (c) For uniaxial extensional flow (UEF) there is equal compression along the  $y$ -axis and  $z$ -axis, and extension along the  $x$ -axis; (d) For biaxial extensional flow (BEF) there is equal extension along the  $y$ -axis and  $z$ -axis and compression along  $x$ -axis. Note that for both planar flows (PCF and PEF) the velocity gradient in the  $\hat{n}_z$  direction is zero.

### Constitutive Equations

The form of the constitutive equation in (2.10) is certainly not the only form possible. In general a functional is required  $P(t) = P[\mathbf{u}(t')]$ , which is dependent on the past history of the velocity of the fluid ( $-\infty < t' \leq t$ ). An example of this more general case is the integral form,

$$\boldsymbol{\sigma}(\mathbf{r}, t) = \int_{-\infty}^t \eta_M(t-t') \dot{\boldsymbol{\gamma}}(\mathbf{r}, t') dt', \quad (2.19)$$

where we have defined the strain rate tensor in (2.11). The viscosity  $\eta_M(t-t')$  is a time dependent function known as the Maxwell memory function. This form of the constitutive equation is still linear in the strain-rate tensor.

In particular for the generalised Maxwell model the constitutive equation is,

$$\boldsymbol{\sigma}(\mathbf{r}, t) = \int_{-\infty}^t \left( \sum_{i=1}^{+\infty} a_i \exp[-(t-t')/\tau_i] \right) \dot{\boldsymbol{\gamma}}(\mathbf{r}, t') dt'. \quad (2.20)$$

The sum in brackets is the time dependent viscosity  $\eta(t-t')$ . The sets of coefficients  $a_i$  and  $\tau_i$  need to be suitably chosen from experiment to fit a particular fluid. This series is usually chosen with a finite number of terms. However, for the case with an infinite number of terms, as long as the inverse of the exponents  $\tau_i^{-1}$  are monotonic increasing with  $i$ , this series can be identified as an example of a Dirichlet series [BG91]. This series converges for  $t$  greater than an earlier cut-off. We will see in Section 2.5 that the Rouse model [Rou53, BCAH87] is an example of a molecular model which leads to a constitutive equation of this type.

The breadth of work on constitutive equations is far too great for us to describe in detail here. We note just three further models: the Doi-Edwards model which we discuss in following sections of this chapter has been found to be of the form of the K-BKZ model (named after A. Kane, B. Bernstein, E. Kearsley and L. Zapas. See [BAH87] and references therein), a

single integral model which incorporates some of the principles of convective constitutive equations. We also mention the retarded motion expansion which is essentially a Taylor expansion of the stress function in terms of the strain-rate tensor. In truncating this expansion at second and third order terms one is left with the so called *second order fluid model* and *third order fluid model*. This expansion is used in the following section on the Curtiss-Bird model, it has also been compared in detail with NEMD simulation by Daivis *et al.* [DMT03, DMT07]. There has been significant work to produce constitutive equations which are based on basic physical principles and in particular invariance principles. This work began with the 1950 paper of Oldroyd [Old50, Ari62, BAH87].

### Rheological transport coefficients

In the literature several viscometric functions are commonly used to characterise the rheology of fluids. Official nomenclature can be found in [Dea95]. Here we list the coefficients used in this thesis, assuming the homogeneous flow geometries as we have described above. Firstly the viscosity from (2.10) is carried over to systems where it is no longer independent of strain rate. For PCF this viscosity is defined as,

$$\eta = -\frac{P_{xy} + P_{yx}}{2\dot{\gamma}}, \quad (2.21)$$

where  $P_{xy}$  and  $P_{yx}$  are both off-diagonal components of the pressure tensor. Far from equilibrium and in particular for polymeric liquids under PCF the diagonal components become unequal, leading to *normal stresses*. In these situations the first and second normal stress coefficients are respectively,

$$\Psi_1 = \frac{P_{yy} - P_{xx}}{\dot{\gamma}^2} \quad (2.22)$$

and

$$\Psi_2 = \frac{P_{zz} - P_{yy}}{\dot{\gamma}^2}. \quad (2.23)$$

For extensional flows only the diagonal components play a role. The zero nature of the off-diagonal components can be justified in the Newtonian regime from the symmetry of the flow through Curie's principle [dGM84]. For PEF we use two viscosities. The first extensional viscosity is,

$$\eta_1 = \frac{P_{yy} - P_{xx}}{\dot{\epsilon}}. \quad (2.24)$$

The second extensional viscosity is,

$$\eta_2 = \frac{P_{yy} - P_{zz}}{\dot{\epsilon}}. \quad (2.25)$$

Substitution of the relevant components of the Newtonian constitutive equation (2.10), with the strain rate tensor chosen for PEF, into the definition of  $\eta_1$  gives the relation  $\eta_1 = 4\eta$ . The ratio  $T_R = \eta_1/\eta = 4$  is the Trouton ratio for PEF; the equivalent relation for UEF  $T_R = \eta_1/\eta = 3$  (see Exercise 1B.1 in [BAH87]) was found by Trouton in 1906 [Tro06, Pet06b]. In comparing PCF and PEF it is convenient to define an extensional viscosity,

$$\bar{\eta} = \frac{\eta_1}{4} = \frac{P_{yy} - P_{xx}}{4\dot{\epsilon}}. \quad (2.26)$$

This definition ensures that close to equilibrium the extensional and shear viscosities converge.

We use the notation above to describe the steady-state transport coefficients in a flow where any transient stresses have diminished. In this chapter we also use the transient viscosities and normal stresses  $\bar{\eta}^+(t)$ ,  $\Psi_1^+(t)$ ,  $\Psi_2^+(t)$  and  $\bar{\eta}^+(t)$ ,  $\eta_1^+(t)$  and  $\eta_2^+(t)$  to describe the corresponding viscosities during the start-up of constant homogeneous flow.

### Extensional Flow

The experimental characterisation of liquids under extensional flows has been particularly challenging for rheologists. This is illustrated in particular by a series of extensional experiments, carried out by different groups, on the same material, which resulted in very divergent results. These experiments were known as the “*M1*” experiments [Wal90, JW94]. The key characteristic which makes these measurement difficult is the exponential nature of extensional flows which can be illustrated by the finite strain tensor,

$$\mathbf{E}(t, 0) = \text{diag}(\exp[+\dot{\epsilon}t], \exp[-\dot{\epsilon}(1+m)t], \exp[+\dot{\epsilon}mt]). \quad (2.27)$$

This flow causes fluid samples to quickly become thin, stretched and fragile. A recent historical review of the rheology of extensional flow has been published by Petrie [Pet06b, Pet06a]. A concise source for information on the various techniques of extensional rheology is Macosko [Mac94]. It is important to note that there is relatively more experimental data on UEF than PEF, however the extensional flows of polymeric liquids still have features in common; in particular, the dominance of strain hardening behaviour, which is the increase of the viscosity with strain-rate.

Many of the methods for extensional rheometry were developed by Munstedt, Laun, Meissner and coworkers [Mac94, TW98]. We begin with the lubricated squeezing flow method, first suggested by Chatraei *et al.* [CMW81], which involves placing a sample in a channel with a ‘U’ shaped cross-section and compressing the sample from above, producing a planar extensional flow. The channel is lubricated so that the friction with the sample has less effect on the flow. Experiments performed using this technique include those of Nishioka *et al.* [NTM<sup>+</sup>00, NTM<sup>+</sup>98, KL91]. Converging flow rheometry (CFR), in which a solution is forced under pressure into a specially shaped die has been used by Jones *et al.* [JWW87] to obtain planar extensional

viscosities of a solution.

Similar methods to CFR have been used in several experimental works over the past fifteen years or so, where DNA molecules and actin filaments in solution are observed using fluorescence microscopy. These experiments have been performed in various planar flows [Sha05]. Perkins *et al.* [PSC94b] have made observations of individual DNA molecules in the start-up of PEF at the stagnation point of a cross-slot flow cell. They were able to test the idea [dG74] that molecules underwent a coil-stretch transition at a critical strain rate. They found that there was a critical behaviour in the steady-state of the conformation. However, contrary to expectation, the dynamics of individual molecules, before steady-state is reached, is very diverse. In the same paper by de Gennes [dG74] hysteresis in the coil/stretch conformations was proposed. In a work subsequent to that of Perkins *et al.* and using similar experimental methods, Schroeder *et al.* [SBSC03] have been able to observe this hysteresis in DNA molecules. Further discussions of rheological experiments using these techniques and theory of these systems is given by Shaqfeh [Sha05]. In Section 2.5.2 we briefly discuss some of the experiments which have been performed, using fluorescence microscopy, to observe equilibrium dynamics of polymers in concentrated solutions.

There have been considerably more experimental investigations of uniaxial extension than planar extensional flow; indeed as we have mentioned above, the first investigations of extensional rheology were of UEF. Various techniques have been used, however, we discuss just one: the filament-stretching technique which has been reviewed by McKinley and Sridhar [MS02]. The filament-stretching rheometer involves placing a sample of viscous fluid between two plates and then stretching the sample by separating the plates. As the process takes place, a filament of the liquid is formed. The radius of the filament decreases exponentially while its length increases exponentially. The extensional viscosity of the sample is calculated after

measuring the width of the filament at the midpoint between the plates as well as measuring the force exerted on one of the end plates. The operation of this device can be tailored to ensure that a homogeneous UEF profile is produced in the sample. McKinley and Sridhar emphasise that this method of rheometry allows for the full history of the sample at the midpoint of the sample to be known, whereas in other techniques the fluid may have a complex and unknown flow history. This is important considering that viscoelastic materials have an intrinsic history dependence.

## 2.4 Polymers and polymeric materials

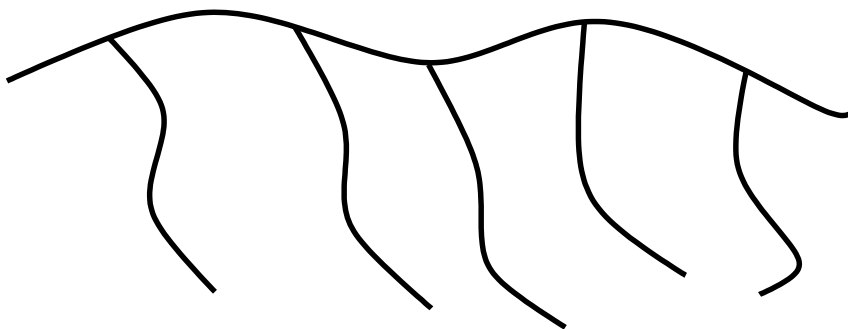
Polymeric materials have a large range of physical properties [Mt03, Spe06, Bil84] which together with the relative economy of their production makes them extremely useful. Polymers are molecules consisting of chains of repeated subunits called monomers, and on a larger scale these chains can be bonded together giving numerous architectures, such as: linear, branched (dendritic) and comb, as depicted in Fig. 2.2. In the bulk concentrated state polymeric materials can be crystalline or glassy, producing some of the most wear resistant materials available. Crosslinked networks of polymer molecules produce elastic rubbers. However, during their production plastics are invariably a liquid melt at some point in the process. Also of interest are polymers in solution which are of importance to molecular biology, while for industrial applications producing dramatic modification of the rheological properties of a liquid.

Two examples of the chemical structure of polymers are given in Fig. 2.3. Both of these; polyethylene and polystyrene are hydrocarbons, consisting of a chain of bonded carbon atoms, with hydrogen atoms or functional groups also bonded to the carbon. In the case of polystyrene, a benzene group takes the place of every fourth hydrogen atom.

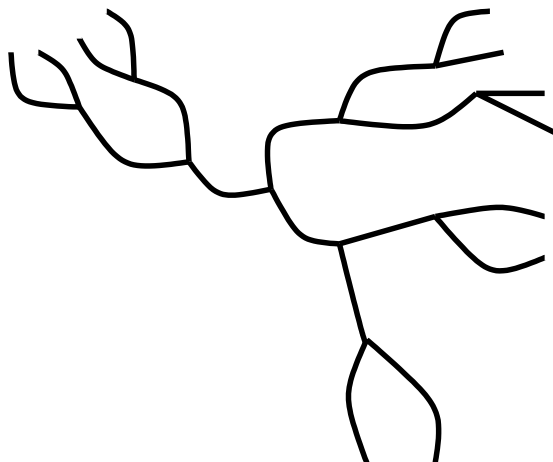
To give an indication of the length of polymer molecules in commercial



(a)



(b)



(c)

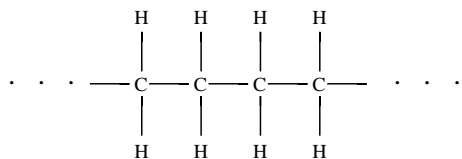
Figure 2.2: A selection of different polymer architectures: (a) is a linear polymer; (b) is a comb polymer and (c) is a branched or dendritic polymer

materials, we cite Sperling [Spe06], who provides examples of the characteristic chain length of polyethylene and the corresponding materials under ambient conditions: with 50 – 1000 carbon atoms per chain, polyethylene is a semi-crystalline solid; with 1000 – 5000 carbon atoms per chain, a tough plastic solid; while with  $3 - 6 \times 10^5$  carbon atoms per molecule polyethylene is used to produce fibres. The final product in each of these cases is a solid. When chain branching occurs, the first carbon of a branch bonds with a carbon of the ‘primary’ chain in place of one of the hydrogen atoms, in the same way as the carbon-carbon bond to the Benzene groups takes place of hydrogen-carbon bonds in polystyrene (Fig. 2.3 (b)). Branching in polyethylene materials distinguishes the commonly used low density polyethylene (more branches) and high density polyethylene (very few branches).

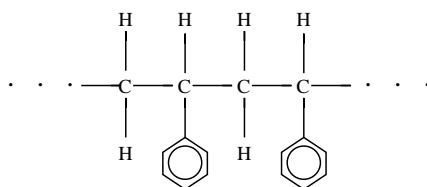
The polymerisation process, in which monomer molecules react to form chain molecules, is itself a statistical process leading to a melt of molecules with a distribution of lengths [BP93]. This property is known as polydispersity. To simplify calculations for analytic models and computer simulations it is common to make the assumption that the molecules have a single characteristic length, making the melt monodisperse. The models we consider in this chapter and which we simulated only consisted of monodisperse systems.

Given that a macroscopic sample of a polymeric liquid consists of large numbers of molecules, it is impossible to consider models of these systems which take into account all of their detail, down to the electronic scale. At this point a suitable level of coarse-graining is required to effectively model polymeric molecules. Coarse-graining refers to the modelling of a system by removing or ignoring degrees of freedom which do not have a large effect on the dynamics and structure of the molecules. This issue is of importance both to analytic models which we consider in this chapter and to interpretation of the molecular models which we use in the next chapter (see Section 3.3.1).

An initial model which considers some of the detail of the bond in the



(a) Polyethylene



(b) Polystyrene

Figure 2.3: The basic form of two polymers; (a) polyethylene and (b) polystyrene. Each of these ‘excerpts’ corresponds to two monomers of that molecule. As indicated by the dots these structures are continued to the left and right.

molecule is the *rotational isomeric state model* (RIS) [BP93, BCAH87]. In this model a molecule is represented as a chain of beads, in place of carbon atoms, between which the bond length and azimuthal bond angle is fixed, while the torsional angle has discrete fixed states (commonly three). The bond is represented by a massless rod. These features are close to the experimental observations. In particular, the torsional fixed states incorporate the observation that, while a torsional potential is smooth, it has well defined minima.

The RIS model may be further coarse-grained by allowing the torsional angle to have any value; this model is known as the Porod-Kratky model [BCAH87]. Allowing, in addition, the bending angle to have any value leads to the *freely jointed chain model*. At this point the models allow beads to intersect, having no accommodation for the effects of excluded volume. This makes the model equivalent to a random flight with fixed step length [Hug95]. It is reasonably straight-forward to calculate the mean squared

end-to-end distance: given a chain with  $N$  beads, if successive bonds of a polymer chain  $\hat{\mathbf{r}}_i$  are randomly oriented but have a constant length  $b_0$  then each chain has an end to end vector,

$$\mathbf{R}_{\mathbf{e}-\mathbf{e}} = \sum_{i=1}^{N-1} b_0 \hat{\mathbf{r}}_i. \quad (2.28)$$

From this definition the length squared of this vector is,

$$R_{e-e}^2 = \mathbf{R}_{\mathbf{e}-\mathbf{e}} \cdot \mathbf{R}_{\mathbf{e}-\mathbf{e}} \quad (2.29)$$

$$= \sum_{i=1}^{N-1} \sum_{j=1}^{N-1} b_0^2 \hat{\mathbf{r}}_i \cdot \hat{\mathbf{r}}_j. \quad (2.30)$$

In this model the bond vectors  $\hat{\mathbf{r}}_i$  are independent of each other, so that for the average over an ensemble of many chains we have  $\langle \hat{\mathbf{r}}_i \cdot \hat{\mathbf{r}}_j \rangle = I_{ij}$  which leads to the result [DE86, Hug95],

$$\langle R_{e-e}^2 \rangle = (N-1)b_0^2. \quad (2.31)$$

Unlike many microscopic quantities the radius of gyration  $R_g$  can be measured in experiment [BP00] and so it is useful to calculate this quantity for comparison with experiment. The radius of gyration of a rigid body with mass  $M$  is defined in terms of the moment of inertia as  $I = MR_g^2$  [Gol80] *i.e.*,  $R_g$  is the radius of the spherical shell with mass  $M$  which has the same moment of inertia as the molecule. If the chain consists of beads of equal mass positioned at the points  $\mathbf{R}_i$ , then the expression for the mean squared radius of gyration is given by,

$$\langle R_g^2 \rangle = \frac{1}{2N^2} \sum_{i=1}^N \sum_{j=1}^N \langle (\mathbf{R}_i - \mathbf{R}_j)^2 \rangle. \quad (2.32)$$

This gives for the freely jointed chain [Hug95],

$$\langle R_g^2 \rangle = \frac{1}{6} N b_0^2 \left( 1 - \frac{1}{N^2} \right). \quad (2.33)$$

As  $N$  becomes large this approaches

$$\langle R_g^2 \rangle = \frac{1}{6} N b_0^2 = \frac{1}{6} \langle R_{e-e}^2 \rangle. \quad (2.34)$$

Both quantities  $\langle R_{e-e}^2 \rangle$  and  $\langle R_g^2 \rangle$  give a measure of the extension of a molecule.

To relate these ideas to the geometry of real linear polymers, we first note that the scalar product (correlation)  $\langle \hat{\mathbf{r}}_i \cdot \hat{\mathbf{r}}_j \rangle$  is not independent of  $i$  and  $j$ . For the correlation to be close to zero the distance along the chain  $|i - j| b_{mol}$  should be greater than some cut-off. We use  $b_{mol}$  here as the bond length of the real molecule to distinguish it from that of the model molecule. The behaviour is often described by the relation  $\langle \hat{\mathbf{r}}_i \cdot \hat{\mathbf{r}}_j \rangle = \exp(-|i - j| b_{mol} / l_p)$ . The length  $l_p$  in this expression is known as the persistence length. In a similar way the dependence of  $\langle \mathbf{R}_{e-e}^2 \rangle$  on the chain length changes so that  $\langle \mathbf{R}_{e-e}^2 \rangle = C_N (N - 1) b_{mol}^2$ , where  $C_N$  is called the characteristic ratio, and is different from unity for non-ideal chains. As  $N$  becomes large the characteristic ratio approaches  $C_\infty$ . Kuhn [Kuh34] introduced a method of coarse-graining a chain molecule by representing it as a freely jointed chain with a suitably chosen bond length  $b_K$ , such that the end-to-end distance of both chains is equal when they are both fully stretched. This means that,

$$b_K = \frac{\langle R_{e-e}^2 \rangle}{R_{e-e}^{(max)}} = \frac{\langle R_{e-e}^2 \rangle}{(N - 1) b_{mol}} = C_\infty b_{mol}. \quad (2.35)$$

The last equality holds when the chain length is large enough to ensure that  $C_\infty$  is a good approximation.

Also of significance is the effect of excluded volume on the scaling relations described above. Analytic or numerical calculations for models of

large chains is a very difficult task even for polymers which lie on a lattice [Sok95]. The main result that we mention here is that models which include the excluded volume lead to  $\langle R_{e-e}^2 \rangle$  scaling with  $N^{2\nu}$  with  $\nu > 1/2$  [DE86]. We describe the geometry of polymers in a melt in Section 2.5.2 where the Doi-Edwards model is introduced.

From the macroscopic perspective, a motivating factor for the development of coarse-grained models has been the observation that some rheological properties are independent of chemical details of the liquid. In particular, the steady-state viscosity was found to have scaling relations independent of the specific chemical. This relation is [DE86, BF68]

$$\eta(M) = \begin{cases} \eta(M_c) \frac{M}{M_c} & \text{for } M < M_c \\ \eta(M_c) \left(\frac{M}{M_c}\right)^{3.4} & \text{for } M > M_c. \end{cases} \quad (2.36)$$

Where  $M_c$  is the molecular weight at which the crossover between the two power laws occurs.

## 2.5 Molecular models for polymer rheology

In Chapter 5 we study the diffusive process in polymeric liquids under planar Couette flow and planar extensional flow. These properties have been studied in conjunction with the viscoelastic properties of the systems in Chapter 4 – many of which we have already described above in the sections on Rheology. The interest in this comparison arises from the relationship which is already known to exist between diffusion and viscoelastic properties of these systems at equilibrium. The understanding of this relationship has come about in particular from kinetic theory of these systems which use principles of statistical mechanics to calculate the properties of these systems.

Kinetic theory and statistical mechanics give important fundamental

principles governing these systems at the molecular scale. These principles include: the concepts of statistical ensembles, Liouville's equation, Boltzmann's equation, *etc.* Combined with the computing resources that we have at hand today, these statistical principles can be used to yield excellent predictions of the properties of polymeric liquids. Methods which we include in this class are: the Monte Carlo technique based on the Metropolis algorithm, equilibrium molecular dynamics simulations and—the main tool of later chapters of this thesis—nonequilibrium molecular dynamics.

In counterpoint there is a large body of literature which deals with polymeric liquids as their sole focus and relies on assumptions about the most important dynamic behaviours to include so as to closer model these systems. One advantage of this approach has been its selective nature which can make the reason for closer match between experiment and theory clearer. On the other hand these methods have historically used less computational resources, thus limiting the level of complexity which can be included in the model and still yield useful, accurate or exact results. However, these models which were originally calculated or solved by hand have recently lead to equivalent stochastic and Brownian dynamics simulations.

The remainder of this chapter is devoted to these models which we term *analytic* to distinguish them from the methods we might call *brute force*. The analytic models presented here with most depth are the Rouse model, Doi-Edwards model and the Curtiss-Bird model. From the last of these we have produced predictions for viscoelastic properties of a monodisperse linear polymer melt under PEF; and to our knowledge this is the first time that this calculation for PEF has been performed.

### 2.5.1 The Rouse Model

Here we briefly consider the Rouse model [Rou53] which was developed to reproduce some of the features of polymers in a dilute solution. The

model's results may also be applied to the short-time dynamics of molecules in polymer melts [DE86], as well as concentrated solutions of short molecules [KG90]. These three situations emphasise the applicability of the Rouse model to situations where the dynamics is not affected by entanglements.

The Rouse model [Rou53] describes a chain of  $N$  beads connected by Hookean springs with a force constant  $k$ , related to the temperature of the system  $T$  and the average bond length  $b$  as follows,

$$k = \frac{3k_B T}{b^2}. \quad (2.37)$$

The coefficient  $k_B$  is Boltzmann's constant. The equations of motion can be written as a coupled set of Langevin equations [Rou53, DE86, BP00],

$$\zeta \dot{\mathbf{r}}_i = -k(\mathbf{r}_{i-1} - 2\mathbf{r}_i + \mathbf{r}_{i+1}) + \mathbf{F}_i^{(\text{rand.})} \text{ for } 1 < i < N, \quad (2.38)$$

$$\zeta \dot{\mathbf{r}}_1 = -k(\mathbf{r}_1 - \mathbf{r}_2) + \mathbf{F}_1^{(\text{rand.})}, \quad (2.39)$$

$$\zeta \dot{\mathbf{r}}_N = -k(\mathbf{r}_{N-1} - \mathbf{r}_N) + \mathbf{F}_N^{(\text{rand.})}. \quad (2.40)$$

Here  $\zeta$  is a friction coefficient which is calculated from the Stokes force on a sphere.  $\mathbf{F}_i^{(\text{rand.})}$  are random forces on each bead in the molecule. This force is due to thermal collisions of solvent molecules with the bead. Results may be obtained from this set of coupled equations by introducing  $N$  normal coordinates, in this context referred to as Rouse modes. Each configuration of the beads in the system can be represented as a linear combination of these modes. Perturbed from an equilibrium configuration each mode will relax with a time constant [DE86],

$$\tau_p = \frac{\tau_R}{p^2} = \frac{\zeta N^2 b^2}{3\pi^2 k_B T} \cdot \frac{1}{p^2}. \quad (2.41)$$

Here  $1 \leq p \leq N$ , while  $\tau_R$  is known as the Rouse time and is the longest time constant in the system. From the modes one is able to calculate the

correlation function for the end-to-end vector,

$$\langle \mathbf{R}_{e-e}(t) \cdot \mathbf{R}_{e-e}(0) \rangle = Nb^2 \sum_{j;\text{odd}} \frac{8}{j^2\pi^2} \exp[-j^2t/\tau_R]. \quad (2.42)$$

We discuss correlation functions in more depth in Chapter 5. A fit of experimental or detailed simulation data to this function should give a value for the Rouse time  $\tau_R$ . The Rouse model also gives a constitutive equation for the stress. This is,

$$\sigma(\mathbf{r}, t) = \eta_s \dot{\boldsymbol{\gamma}}(\mathbf{r}, t) + \int_{-\infty}^t nk_B T \sum_{p=1}^{+\infty} \exp[-2(t-t')p^2/\tau_R] \dot{\boldsymbol{\gamma}}(\mathbf{r}, t') dt' \quad (2.43)$$

where  $\eta_s$  is the solvent viscosity and  $n$  is the monomer concentration. Apart from the addition of the term due to the solvent viscosity, this constitutive equation has the same form as the generalised Maxwell model (2.20).

The constitutive equation (2.43) can be directly integrated to give a constitutive equation for the start-up of PCF and PEF. Integration to  $t = +\infty$  gives an intrinsic steady state viscosity,

$$[\eta] = \lim_{\rho \rightarrow 0} \frac{\eta - \eta_s}{\rho \eta_s} = \frac{N_A}{M \eta_s} \frac{N^2 b^2 \zeta}{36}. \quad (2.44)$$

Here  $\rho$  is the density of polymer in the solution and  $N_A$  is Avogadro's number. The main result here is that the intrinsic viscosity is proportional to molecular weight  $M$ . For the same species of polymer, this corresponds to a proportionality with the polymer length  $N$ . The other result of the model significant to this thesis is its prediction for the diffusion coefficient,

$$D_G = \frac{k_B T}{N \zeta}; \quad (2.45)$$

The diffusion coefficient is inversely proportional to molecular length.

The Rouse model is just a first step in the prediction of the properties

of linear molecules in solution. For example, the model does not include the *hydrodynamic interaction*, *i.e.*, the forces on beads from the motion of solute which itself is due to motion of the chain. This effect was first included in the Zimm model [Zim56]. This lead to adjusted predictions for the chain length dependence of  $D$  and  $\eta$ . Further assumptions, such as the infinite extensibility of the bonds in the Rouse chain, are removed in numerous other models considered in the literature. A good source for information on these models is the volume by Bird *et al.* [BCAH87].

### 2.5.2 The Doi-Edwards Model

Moving on from the rheology of solutions, the model of Doi and Edwards [DE78a, DE78b, DE78c, DE86] provides a constitutive equation for a polymer melt. The model is based on assumptions of how molecules diffuse in a melt, assumptions of how molecules contribute to the stress in the fluid as well as assumptions of how the structure of the system should be coarse-grained. The central ideas about the diffusion of a ‘test’ molecule in a polymer melt were introduced by de Gennes [dG71]. In this model de Gennes assumed that the test molecule was able to diffuse parallel to its contour but was unable to diffuse in the transverse direction due to the surrounding molecules forming a mesh. However, at its ends the molecule is assumed to be free to diffuse in any direction.

Borrowing from the theory of rubber elasticity [Edw67], the initial constraints on the chain are conveniently represented by a tube (see Fig. 2.4 (a)). As one chain end explores new regions of the melt, the other end diffuses within the tube. Thus, the unoccupied tube is no longer a constraint. In this way the portion of the original tube which is still occupied by the molecule decreases with time (Fig. 2.4 (b)-(e)). The forward and backward diffusion is reminiscent of the motion of a snake and for this reason the motion was given the name reptation by de Gennes, after the Latin word

*reptare*, which means to creep.

Along with the use of the tube method, the structure of the polymer melt is coarse-grained by assuming that the test polymer may be represented by a primitive path. The primitive path of the polymer is the path between its two ends which has the shortest length, while keeping the same topology. This means that the primitive path of the test molecule and the test molecule itself have the same molecules constraining their motion. It is also assumed that the primitive path has constant length  $L$ , and that it may be represented as a Rouse chain with the Hookean spring constant given by (2.37). The chain is assumed to be Gaussian and so the mean-squared distance between points on the chain is given by,

$$\langle (\mathbf{R}(s', t) - \mathbf{R}(s, t))^2 \rangle = a|s' - s|. \quad (2.46)$$

Where  $\mathbf{R}(s, t)$  and  $\mathbf{R}(s', t)$  are the positions at time  $t$  of the points on the primitive path parameterised by  $s$  and  $s'$  which are a distance  $|s - s'|$  apart along the contour of the primitive path. The parameter  $a$  is called the step-length of the chain. Considering the two ends of the chain  $s = 0$  and  $s' = L$ , this leads to the identity,

$$Nb^2 = La. \quad (2.47)$$

Having summarised the structural properties of the chain and its parameterisation, we can now quote some of the dynamic properties in terms of these parameters: the fraction of chain which still remains in the original tube after a time  $t$  is given by the function,

$$\psi(t) = \sum_{p:\text{odd}} \frac{8}{p^2\pi^2} \exp[-p^2t/\tau_d]. \quad (2.48)$$

In this expression the constant  $\tau_d$  is the so called disengagement time and

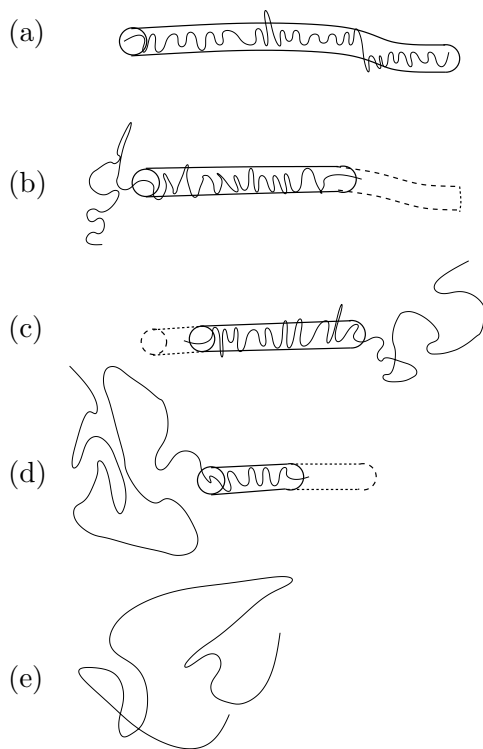


Figure 2.4: Reptation and disengagement of a molecule. (a) The initial constraints on a polymer in a melt are represented by a tube. (b)-(d) As the molecule diffuses through a polymer melt, diffusion along the primitive path of the molecule—known as reptation—is most significant. In time the portion of the initial tube which is still populated by the molecule decreases until, (e) the initial tube contains no part of the molecule (after Fig. 3 in [Gra82]).

is given in terms of model parameters as,

$$\tau_d = \frac{\zeta N^3 b^2}{\pi^2 k_B T} \left( \frac{b}{a} \right)^2. \quad (2.49)$$

In making the calculation of (2.48) it is assumed that the one-dimensional diffusion along the contour of the primitive path has the diffusion coefficient given by the Rouse model (2.45).

De Gennes found that the reptation model predicted a diffusion coefficient for the molecule's centre of mass to be proportional to  $M^{-2}$ . While reptative motion has been seen in simulations of chain molecules, results we will discuss further in Chapter 5, direct observations of reptation have been made by Käs *et al.* [KSS94] and Perkins, Smith and Chu [PSC94a, SPC95]. In the work of Käs *et al.* the reptative motion of fluorescently labelled actin filament was observed in a solution of similar but unlabelled molecules. While in the work of Perkins, Smith and Chu, labelled DNA molecules were observed to reptate.

In this model it is assumed that the stress in a polymeric liquid is solely due to the forces along the chain of a molecule.

$$\sigma_{\alpha\beta}(t) = \frac{c}{N} \sum_n \frac{3k_B T}{b^2} \left\langle \frac{\partial R_{n\alpha}}{\partial n} \frac{\partial R_{n\beta}}{\partial n} \right\rangle \quad (2.50)$$

The partial derivatives represent components of the tangent vector to the chain,  $n$  is the coordinate along the contour of the chain and  $R_{n\alpha}$  is the Cartesian coordinate  $\alpha$  of the chain at that point. The factor  $\frac{3k_B T}{b^2}$  is the force constant for the Hookean spring (2.37),  $c$  is the polymer number density. The main supporting evidence for this form of the stress tensor (2.50) is the stress-optic rule [DE86], an important result from optical birefringence experiments, which shows that the stress tensor is proportional to the alignment tensor for the melt. The expression for the stress tensor corresponds to part of the full virial term of the stress tensor [McQ76]. This is seen by

comparing with the expression for the stress tensor described at the end of the next chapter (3.28) and used in our molecular dynamics simulations of chain molecules.

As the end of a chain leaves its tube at time  $t'$ , it orients randomly in a direction  $\hat{\mathbf{u}}$ , and then due to the flow begins to change direction under the affine transformation  $\mathbf{E}(t, t')$ . At a later time  $t$  this new tube segment makes the following contribution to the stress tensor,

$$\frac{c}{N} \frac{3k_B T L^2}{N b^2} \left( \frac{(\mathbf{E}(t, t') \cdot \hat{\mathbf{u}})_\alpha (\mathbf{E}(t, t') \cdot \hat{\mathbf{u}})_\beta}{|\mathbf{E}(t, t') \cdot \hat{\mathbf{u}}|^2} - \frac{1}{3} I_{\alpha\beta} \right) \quad (2.51)$$

with probability,

$$dt' \left( \frac{\partial}{\partial t'} \psi(t - t') \right) \quad (2.52)$$

It is assumed in (2.51) that sections of the chain (which has constant length) align independently. This is called the independent alignment approximation and is denoted with a superscript ( $IA$ ). We discuss the approximation further on page 38. Averaging over the uniform distribution of  $\hat{\mathbf{u}}$  one obtains the constitutive equation,

$$\sigma_{\alpha\beta}(t) = G_e \int_{-\infty}^t dt' \left( \frac{\partial}{\partial t'} \psi(t - t') \right) Q_{\alpha\beta}^{(IA)}(\mathbf{E}(t, t')) \quad (2.53)$$

The factor  $G_e$  is the plateau modulus and is given in terms of geometric properties by

$$G_e = \frac{c}{N} \frac{3k_B T L^2}{N b^2} \quad (2.54)$$

The elements of the order tensor  $Q^{(IA)}$  are

$$Q_{\alpha\beta}^{(IA)} = \left\langle \frac{(\mathbf{E} \cdot \hat{\mathbf{u}})_\alpha (\mathbf{E} \cdot \hat{\mathbf{u}})_\beta}{|\mathbf{E} \cdot \hat{\mathbf{u}}|^2} - \frac{1}{3} I_{\alpha\beta} \right\rangle_o \quad (2.55)$$

where the angled brackets denote the integral over the unit sphere. We followed the work of Bird *et al.* [BSC82a], using their choice of spher-

ical coordinate scheme:  $(x, y, z) = (r \cos \phi, r \cos \theta \sin \phi, r \sin \theta \sin \phi)$ , here  $\theta$  is measured from the  $z$ -axis, while  $\phi$  is measured from the  $x$ -axis. In these coordinates the integral denoted by the angled brackets is given by  $\langle \dots \rangle_o = \frac{1}{4\pi} \int (\dots) d\hat{\mathbf{u}} = \frac{1}{4\pi} \int_0^\pi \int_0^{2\pi} (\dots) \sin \phi d\theta d\phi$ .

The derivative of  $\psi(t)$  is often written as a separate function,

$$\frac{\partial \psi(t-t')}{\partial t'} = \frac{8}{\pi^2 \tau_d} \sum_{p, \text{odd}} \exp[-p^2(t-t')/\tau_d] \quad (2.56)$$

For numerical purposes it is useful to transform this function using the Poisson summation formula [BSC82a, MF53] to give,

$$\frac{\partial \psi(t-t')}{\partial t'} = \frac{2}{\pi^2 \tau_d} \left( \frac{\pi \tau_d}{t-t'} \right)^{1/2} \sum_{n=0, \pm 1, \pm 2, \dots} (-1)^n \exp \left[ -\frac{n^2}{4} \frac{\pi^2 \tau_d}{(t-t')} \right] \quad (2.57)$$

Furthermore (2.56) may be written in terms of the Jacobi Theta function [WW96],

$$\Theta_2(z | \tau) = 2 \exp[i\pi\tau/4] \sum_{n=0}^{+\infty} \exp[i\pi\tau(n^2 + n)] \cos[(2n+1)z], \quad (2.58)$$

as,

$$\frac{\partial \psi(t-t')}{\partial t'} = \frac{4}{\pi^2 \tau_d} \Theta_2 \left( 0 \left| \frac{4i(t-t')}{\pi \tau_d} \right. \right). \quad (2.59)$$

### Calculation under planar extensional flow.

Predictions of the DE-model for PCF have been calculated in the paper by Doi and Edwards [DE78d], and independently as part of the Curtiss-Bird calculation for their model [BSC82b]. The results for the ratio of the steady-state viscosity to the zero strain-rate viscosity are reproduced in Fig. 2.7. In this section we show how the corresponding predictions of the DE-model for PEF may be calculated. In particular we have calculated the ratio between the steady-state extensional viscosity and the zero strain-rate value  $\bar{\eta}(\dot{\epsilon})/\bar{\eta}(0)$ .

The steady-state viscosity is calculated from the model in the limit as  $t \rightarrow +\infty$  after the start-up of homogeneous flow. For the start-up of PEF the deformation gradient is given by,

$$\mathbf{E}(t, t') = \text{diag}(\exp[\dot{\epsilon}(t - t')], \exp[-\dot{\epsilon}(t - t')], 1)H(t - t'), \quad (2.60)$$

where  $H(t)$  is the Heavyside step function. Following Curtiss *et al.* [BSC82a], on substitution of (2.60) into (2.53) and simplification using integration by parts we obtain,

$$\bar{\eta}(\dot{\epsilon}) = \frac{G_e}{4\dot{\epsilon}} \int_0^{+\infty} dt \left( \frac{\partial}{\partial t'} \psi(t - t') \right) \Big|_{t'=0} \left( Q_{xx}^{(IA)} - Q_{yy}^{(IA)} \right) \Big|_t \quad (2.61)$$

where the order tensor term is given by,

$$\begin{aligned} & \left( Q_{xx}^{(IA)} - Q_{yy}^{(IA)} \right) \Big|_t \\ &= \frac{1}{4\pi} \int_0^{2\pi} \int_0^\pi \frac{(\cos^2 \theta - \sin^2 \theta \sin^2 \phi) \sin \theta d\theta d\phi}{[1 + (\Lambda(t)^2 - 1) \sin^2 \theta \sin^2 \phi + (\Lambda(t)^{-2} - 1) \cos^2 \theta]^{3/2}} \end{aligned} \quad (2.62)$$

and  $\Lambda(t) = \exp(\dot{\epsilon}t)$ . Care must be taken in evaluating this integral around  $\Lambda = 1$  *i.e.* around  $\dot{\epsilon}t = 0$ . We have found by performing a Taylor expansion of the integrand in  $\dot{\epsilon}t$  and then performing the spherical integration symbolically using Mathematica, that around  $\dot{\epsilon}t = 0$  the integral has the Taylor expansion,

$$\left( Q_{xx}^{(IA)} - Q_{yy}^{(IA)} \right) \Big|_t = (4/5)\dot{\epsilon}t - (8/35)(\dot{\epsilon}t)^3 + (6808/75075)(\dot{\epsilon}t)^5 + \dots \quad (2.63)$$

Doi and Edwards [DE78c] found the zero strain-rate viscosity using the zero frequency limit of the viscosity under oscillatory PCF. We verify here that the same result is found in the limit as  $\dot{\epsilon} \rightarrow 0$  under PEF. From (2.63)

and (2.61) it follows that,

$$\begin{aligned}\bar{\eta}(0) &= \frac{G_e}{5} \int_0^{+\infty} dt \frac{8}{\pi^2 \tau_d} \sum_{p, \text{odd}} t \exp[-p^2 t / \tau_d] \\ &= \frac{G_e \tau_d}{\pi^2} \sum_{p, \text{odd}} \frac{1}{p^4} = \frac{\pi^2}{60} G_e \tau_d = \frac{\zeta c N^3 b^6}{20 a^4}.\end{aligned}\quad (2.64)$$

This is in agreement with the result of Doi and Edwards. The second last equality uses the identity  $\sum_{p, \text{odd}} \frac{1}{p^4} = \frac{\pi^4}{96}$  which can be shown by using the Hurwitz and Riemann zeta functions [SW07]. The last equality may be found by using equations (2.54) and (2.49) for  $G_e$  and  $\tau_d$  respectively and (2.47)  $Nb^2 = La$ . The proportionality of  $\eta(0)$  with  $N^3$  was an important initial success of the DE-model, having closer agreement with the experimental result  $N^{3.4}$ . The further improvement of this agreement with experiment was one of the goals of the many improved tube models which we discuss in the next section.

Away from the zero strain-rate case, the ratio  $\bar{\eta}(\dot{\epsilon})/\bar{\eta}(0)$  was calculated numerically using Mathematica and results for the full integral (2.62) are shown in Fig. 2.9. These results show that the DE-model we have presented predicts only thinning under PEF. This is also the general behaviour of the model for UEF [DE78d]. At the time of publication Doi and Edwards found that there was not enough agreement amongst experimental results to make a judgement about any comparison with the model. However, there is now agreement [Mac94] that under extensional flows polymeric fluids show a region of strain hardening together with a plateau region followed by a region of thinning.

### Further developments of tube based models

The summary of the model that we have presented above is the original Doi-Edwards model. This model, as we have already stated, has been very

influential and has led to models which relax some of the approximations and attempt to remove some of the discrepancies which exist between the DE-model and experimental results. This has resulted in exploration of the effect that details on the molecular scale have on the macroscopic properties.

Some of the dynamics and assumptions which we look at in the following section include: ‘*contour length fluctuation*’, ‘*chain stretching*’, ‘*the independent alignment approximation*’, ‘*constraint release*’ or ‘*double reptation*’, ‘*convective constraint release*’ and ‘*tube anisotropy*’. The name of each of these alone already suggests the aspect being considered. In addition to these specific assumptions there has also been a range of computational methods used to compute the predictions of models and on which to found the models. The Doi-Edwards results which were obtained above used only numerical integration to obtain a result. However, it has been increasingly common to use stochastic methods and simulations which are closer in nature to the molecular simulations which we present in the next chapter.

The relaxation of the assumption that the primitive chain has a fixed length was considered by Doi and Edwards [DE86]. The primitive chain is a coarse-grained model of the actual molecule and thus the primitive chain should have a fluctuating length. That this is the case should also be noted from the assumption that the primitive chain is modelled as a Rouse chain which clearly has a fluctuating length, since each of the bonds fluctuates. It was shown by Doi and Edwards that the inclusion of a fluctuating contour-length in the model would lead to a shorter disengagement time  $\tau_d$  and a consequential increase in the centre-of-mass diffusion coefficient. The consideration of *contour-length fluctuation* led Doi [Doi83] to an improvement of the exponent for the power-law relation between the chain-length and the zero strain-rate viscosity (2.5.2). In several of the subsequent models contour-length fluctuation has been included as just one of the additional properties [Ött99, HS98]. We should also mention that contour-length fluctuation is

significant in systems of branched molecules where reptation is reduced due to the ‘pinning’ of branch points in the melt [DE86, MM98, MM99].

In addition to the thermal fluctuation of the contour-length the model should also include the effect of *chain stretching* due to the flow. Works which have included this effect are those of Marrucci and Grizzuti [MG88a, MG88b] and Mead, Yavich and Leal [ML95, MYL95]. The latter group of authors note that this effect is of particular importance in differentiating between shear and extensional flows.

As we have mentioned above the model assumes that sections of the chain deform independently of each other under the affine transformation  $E(t, t')$ . Relaxing this assumption lead Doi [Doi80, DE86] to a non-linear partial differential equation. There are only some flows for which solutions can be found exactly which makes numerical solutions necessary [Ött89, DE86]. This model was used to improve predictions of double-step experiments where a polymer sample is sheared with an abrupt sequence of step strains in opposite directions. It was concluded [DE86] that the full DE model is required in these cases of large deformations.

The tube in the DE-model represents the constraint by the mesh of molecules which surround the test molecule. To be in some sense self-consistent, the reptative motion of these molecules should also be incorporated into the model. At times these surrounding molecules will move so that they are no longer a constraint to the test molecule. This effect goes by the name of *constraint release* or *double reptation* and has been considered specifically in the works of des Cloizeaux [dC88] and Tsenoglou [Tse87]. This process has recently been observed experimentally by Zamponi *et al.* [ZWM<sup>+</sup>06] in blends of polyethylene using neutron spin echo spectroscopy. By varying the length of host molecules in their sample the affect of constraint release could be observed.

In addition to the diffusive constraint release, under flow there is relative

motion of molecules due to the velocity gradient that leads to *convective constraint release*. A series of papers by Marrucci and Ianniruberto considered this effect [Mar96, IM96].

A model of Ianniruberto and Marrucci [IM98, MI99] considers the contribution made to the stress by the interaction of a polymer with the constraints. The model incorporates the deformation of the tube cross-section. It is shown that this contribution is greatest in cases where the cross-section is anisotropic. These ideas have been used and improved upon in the model of Öttinger [Ött99] which uses the GENERIC formalism [Ött05].

There had been considerable debate over the chain-length dependence of the centre-of-mass diffusion coefficient and the zero strain-rate viscosity. Lodge [Lod99] has reexamined experimental results from the literature and performed additional experiments concluding that there was little discrepancy between the power-laws. Lodge summarises the issue in the following way: it was understood that tube theories predicted that  $D \propto \frac{R_g^2}{\tau_d} \propto N^{-2}$  (noting that  $R_G^2 \propto N$  (2.33)) which was in agreement with the original DE-model and was understood to be validated by experiment. However, at the same time the model predicted that the power law dependence for the viscosity was given by,  $\eta_0 \propto \tau_d \propto N^3$  (as we have verified above for PEF (2.64)). Concurrently experiment showed that  $\eta_0 \propto N^{3.4}$ . On the one hand theory required  $\tau_d$  to be altered for viscosity while on the other requiring it be unchanged for diffusion. The conclusion of Lodge was that the experimental result for the power-law was in error, having a revised form  $D \propto N^{-2.3 \pm 0.1}$ , in agreement with theory.

Throughout the second half of this chapter we have introduced several power-law relations for the zero strain-rate viscosity and the diffusion coefficient both in solutions and in melts. These have been gathered together in Table 2.1 along with several others from the literature.

Models like those described above continue to be developed and we admit

Type	Author	Diffusion	Viscosity
		$D \propto \dots$	$\eta_0 \propto \dots$
T	Rouse [Rou53]	$N^{-1}$	$N^1$
T	Zimm ( $\theta$ solvent) [Zim56]	$N^{-0.5}$	$N^{0.5}$
T	de Gennes [dG71]	$N^{-2}$	—
T	Infinite tube [DE78a]	$N^{-2}$	—
T	Doi and Edwards [DE78a, DE78c]	$N^{-2}$	$N^3$
T	Contour-length fluctuation [Doi83]	-	$N^{3.5}$
S	Kremer and Grest [KG90]	$N^{-2.28 \pm 0.05}$	$N^{3.4}$
S	Kröger and Hess [KH00]	—	$N^{3.3 \pm 0.2}$
E	Lodge [Lod99]	$N^{-2.28 \pm 0.05}$	$N^{3.4}$
T	Frischknecht and Milner [FM00]	$N^{-2.25}$	$N^{3.4}$
S	Masubuchi <i>et al.</i> [MTK <sup>+</sup> 01]	$N^{-2.4 \pm 0.2}$	$N^{3.5 \pm 0.1}$

Table 2.1: Theoretical (T) and simulated (S) predictions for the variation of the centre of mass diffusion coefficient  $D$  and the zero strain-rate viscosity  $\eta_0$ . The experimental results of Lodge (E) [Lod99] are also included.

it is difficult to keep up with the various aspects which have been considered and noting in addition that each of the investigations involved significant comparison by the authors with experimental data. The summary above gives an indication of the scope of this field. Significantly it shows more clearly the approximations which are made in the DE-model. Further review of the work proceeding from Doi and Edwards is given by Leal and Oberhauser [LO00].

### Simulations based on the Doi-Edwards model.

Before moving on to the Curtiss-Bird model in the next section, we mention separately several of the numerical models which have grown out of the methods used above. In the first of the series of papers of Doi and Edwards [DE78a] the notion of *slip-links* was used to model the constraining affect of entanglements. In the past decade this explicit, though coarse-grained, model has been used as a basis for numerical simulations of polymer melts [TTD00, TTD01]. Tasaki *et al.* [TTD01] have investigated UEF of polydisperse systems. In a similar way Hua *et al.* [HS98, HSV99, Hua00, HC99,

HK00] have developed a stochastic simulation of polymer melts. Though without explicit slip-links, these simulations determine the motion of a single test molecule with interactions which model the surrounding molecules.

Of this type of simulation, there have been some which have looked at explicit three-dimensional systems of model molecules. Padding and Briels [PB01, PB02, PB03] have simulated a model of polyethylene where 20 consecutive monomers are represented as a blob. The motion of these blobs is governed by a Langevin equation. Entanglements are introduced into the model by explicitly including elastic bond ‘filaments’. Padding and Briels have investigated diffusion in the cross-over region between Rouse and reptation regimes, as well as viscometric functions and alignment in the start-up and steady-state of PCF.

A similar type of simulation was introduced in the ‘NAPLES’ simulations of Masubuchi *et al.* [MTK<sup>+</sup>01]. These simulations represent the polymer melt as an explicit three-dimensional network of primitive chains with entanglements modelled as slip-links. The initial paper [MTK<sup>+</sup>01] investigated properties at equilibrium and had success in predicting the correct exponent for the chain-length dependence of the centre of mass diffusion [Lod99] (See Tab.2.1). Subsequent works, for example by Masubuchi *et al.* [MHG<sup>+</sup>04] and Bruzzone and Malvaldi, [BM06] have also looked at systems under PCF. Using the NAPLES code Bruzzone and Malvaldi [BM06] investigated the effect of the flow on conformational and diffusive properties of the polymer melt. They found that there was an increased diffusivity in all directions due to the flow. This result is significant for the calculations of diffusion which we present in Chapter 5.

### 2.5.3 The Curtiss-Bird Model

We now introduce the model of Curtiss and Bird (CB-model) which was developed in a series of papers by Curtiss, Bird and Saab [CB81b, CB81a,

BSC82a, BSC82b] and presented together in the second edition of volume two of the book *Dynamics of Polymeric Liquids* [BCAH87]. After our introduction of the model we present the calculation and results of the CB-model for PEF.

The method of Bird *et al.* is to use a very general but formal phase-space theory based on Liouville's equation for the time dependence of a phase-space distribution function of all molecules in the system. They then find a continuity equation for the configurational distribution function. This calculation involves integration over the momentum-space coordinates.

The initial assumption of the model for linear molecules is that the polymer melt may be described by Kramers freely jointed bead-rod chains; a coarse-grained model consisting of beads connected by massless rods of length  $a'$ . In the original papers it was assumed that the system was monodisperse with  $N$  beads per chain, while in the book [BCAH87] the system is polydisperse. To make the model tractable, assumptions are made regarding the dynamics and forces on the beads in the chain. These are:

1. A short-range-force approximation: The intramolecular and intermolecular interaction potential between beads is only significant when the beads are very close.
2. An anisotropic Stokes law: Beads experience a Stokes force, a hydrodynamic friction force due to the surrounding molecules. The difference between this force on adjacent pairs of beads is assumed to be anisotropic. The anisotropy is parameterised by the *link tension coefficient*  $0 \leq \epsilon \leq 1$ . If  $\epsilon = 0$  then the differences in these forces is isotropic, while if  $\epsilon = 1$  there is no component of the difference between the forces in adjacent links in the direction of the contour of the molecule. It is also assumed that this difference scales with the length of the chain and is proportional to  $N^\beta$ , where  $\beta$  is a positive parameter.

3. The Brownian motion of chains is anisotropic: it is assumed that there are two contributions to the Brownian motion of a bead, the first is isotropic while the second is an anisotropic Brownian motion parallel to the local contour of the chain, noting that at the chain ends the motion is isotropic. This assumption is similar to the reptation hypothesis of the DE-model. The proportion of the two contributions is parameterised by the *reptation* coefficient  $0 \leq \epsilon' \leq 1$ . If  $\epsilon' = 1$  then the Brownian motion is solely isotropic while if  $\epsilon' = 0$  then there is only reptative motion. The model that we consider below is solely reptative *i.e.*  $\epsilon' = 0$ .
4. The *mild curvature* approximation: This assumes that the change in direction of the contour of a chain is not abrupt. This simplifies calculations by allowing a Taylor expansion to be used in estimating the local variation of the distribution function along the contour of the chain.

Using these assumptions a diffusion equation for the configuration-space distribution function of a single molecule is found. Further calculation leads to a diffusion equation for the single link distribution function. A time constant  $\lambda$  for this equation is defined in terms of the parameters of the model and is given by,

$$\lambda = \frac{N^{3+\beta} \zeta a'^2}{2k_B T}. \quad (2.65)$$

Here  $\zeta$  is the scalar friction coefficient representing the magnitude of the Stokes force presented in assumption 2.  $\lambda$  represents the longest time coefficient for the model.

To obtain a constitutive equation from this model a formal expression is found for the stress tensor of the system in terms of the hydrodynamic force on a molecule and the configuration-space distribution function. This is then formulated in terms of the single-link distribution function. This leads to the

time dependent stress tensor of the Curtiss-Bird model given by,

$$\sigma(t) = NnkT \left[ \frac{1}{3} \mathbf{1} - \int_{-\infty}^t \mu(t-t') \mathbf{A}(t, t') dt' - \epsilon \int_{-\infty}^t \nu(t-t') \mathbf{B}(t, t') dt' \right]. \quad (2.66)$$

Here  $\mu$  and  $\nu$  are memory functions independent of the flow and  $n$  is the number density of molecules. The tensors  $\mathbf{A}$  and  $\mathbf{B}$  are given by,

$$\mathbf{A}(t, t') = \langle \hat{\mathbf{u}} \hat{\mathbf{u}} [1 + \gamma^{[0]}(t, t') : \hat{\mathbf{u}} \hat{\mathbf{u}}]^{-3/2} \rangle_0, \quad (2.67)$$

$$\mathbf{B}(t, t') = \frac{1}{2\lambda} \dot{\gamma}(t) : \langle \hat{\mathbf{u}} \hat{\mathbf{u}} \hat{\mathbf{u}} \hat{\mathbf{u}} [1 + \gamma^{[0]} : \hat{\mathbf{u}} \hat{\mathbf{u}}]^{-3/2} \rangle_0. \quad (2.68)$$

The dependence on the flow arises through the strain-rate tensor  $\dot{\gamma}(t)$  defined in (2.11) and the finite strain tensor  $\gamma_{ij}^{[0]}(t, t') = \sum_m \frac{\partial x'_m}{\partial x_i} \frac{\partial x'_m}{\partial x_j} - I_{ij}$ .  $x_m$  is a Cartesian coordinate at a past time  $t'$  of a material point which at time  $t$  is at position  $x$ . The unit vector  $\hat{\mathbf{u}}$  – unrelated to the streaming velocity – parameterises the distribution of bond vectors in the melt, while  $\langle \dots \rangle_0 \equiv \frac{1}{4\pi} \int_0^{2\pi} \int_0^\pi \dots \sin \theta d\theta d\phi$  represents an average over the unit sphere, as we presented for the DE-model. For PEF,

$$\dot{\gamma}(t) = \text{diag}(+2\dot{\epsilon}, -2\dot{\epsilon}, 0) H(t) \quad (2.69)$$

and the finite strain is given by,

$$\gamma^{[0]}(t, t') = (\exp[-2\dot{\epsilon}t] - 1, \exp[+2\dot{\epsilon}t] - 1, 0). \quad (2.70)$$

The memory functions  $\mu$  and  $\nu$  are independent of the flow and are given by the series,

$$\mu(t-t') = \frac{8}{\lambda} \sum_{p, \text{odd}} \exp[-\pi^2 p^2 (t-t')/\lambda] \quad (2.71)$$

$$\nu(t-t') = \frac{16}{\pi^2 \lambda} \sum_{p, \text{odd}} p^{-2} \exp[-\pi^2 p^2 (t-t')/\lambda]. \quad (2.72)$$

The memory function  $\frac{\partial\psi(t-t')}{\partial t'}$  (2.56) for the DE-model is equivalent to  $\mu(t-t')$  under the parameter change  $\lambda = \pi^2\tau_d$ . As we have stated, Bird *et al.* [BSC82a] note that the function above should be transformed for small values of  $(t-t')$  to give the series over all integers,

$$\mu(t-t') = \frac{2}{\lambda} \left( \frac{\lambda}{\pi(t-t')} \right)^{1/2} \sum_{n=0,\pm 1,\pm 2,\dots} (-1)^n \exp \left[ -\frac{n^2}{4} \frac{\lambda}{(t-t')} \right]. \quad (2.73)$$

The functions  $\mu(t)$  and  $\nu(t)$  are plotted in Figs. 2.5 and 2.6 respectively. It is seen that  $\mu(t)$  diverges as  $t$  approaches zero while  $\nu(t)$  approaches 2 in this limit. Both functions converge monotonically to zero as  $t$  increases. Again we note that these series may be expressed in terms of the Jacobi theta functions.

### Calculation of the Curtiss-Bird model for PEF

Curtiss, Bird and Saab [CB81b, CB81a, BSC82a, BSC82b] used the constitutive equation (2.66) to model the start-up and steady-state properties under PCF and UEF. They looked at viscosities and normal stresses, in some cases fitting the model with experimental results. We have recalculated their results [BSC82b] for steady-state shear viscosity presenting them in Fig. 2.7, plotting  $\eta(\dot{\gamma})/\eta(0)$  against  $\lambda\dot{\gamma}$ . It is seen that the model predicts shear thinning, with a rate dependent on the link-tension coefficient. The aim for the remainder of this section is to present the calculation and results of this model under PEF. To the best of our knowledge this is the first presentation of this calculation in the literature.

It may be found from (2.66) using integration by parts that the transient extensional viscosity has the form,

$$\begin{aligned} \frac{\bar{\eta}^+(t; \dot{\epsilon})}{Nn k T \lambda} &= \frac{1}{4\lambda\dot{\epsilon}} \int_0^t \mu(s)(A_{xx} - A_{yy})|_s ds + \frac{1}{4\lambda\dot{\epsilon}}(A_{xx} - A_{yy})|_t \int_t^{+\infty} \mu(s) ds + \\ &\epsilon \int_0^t \nu(s) \left( \frac{B_{xx} - B_{yy}}{4\lambda\dot{\epsilon}} \right) \Big|_s ds + \epsilon \left( \frac{B_{xx} - B_{yy}}{4\lambda\dot{\epsilon}} \right) \Big|_t \int_t^{+\infty} \nu(s) ds. \end{aligned} \quad (2.74)$$

The required linear combinations of components of the tensors **A** and **B** are given by,

$$\begin{aligned} &(A_{xx} - A_{yy})|_t \\ &= \frac{1}{4\pi} \int_0^{2\pi} \int_0^\pi \frac{(\cos^2 \theta - \sin^2 \theta \cos^2 \phi) \sin \theta d\theta d\phi}{[1 + (\Lambda(t)^2 - 1) \sin^2 \theta \sin^2 \phi + (\Lambda(t)^{-2} - 1) \cos^2 \theta]^{3/2}} \end{aligned} \quad (2.75)$$

$$\begin{aligned} &\left( \frac{B_{xx} - B_{yy}}{\lambda\dot{\epsilon}} \right) \Big|_t \\ &= \frac{1}{\lambda\dot{\epsilon}} \frac{1}{4\pi} \int_0^{2\pi} \int_0^\pi \frac{((\cos^2 \theta - \sin^2 \theta \sin^2 \phi)^2) \sin \theta d\theta d\phi}{[1 + (\Lambda(t)^2 - 1) \sin^2 \theta \sin^2 \phi + (\Lambda(t)^{-2} - 1) \cos^2 \theta]^{3/2}}, \end{aligned} \quad (2.76)$$

where  $\Lambda(t) = \exp(\dot{\epsilon}t)$ . We have calculated the integrals using Mathematica and plot them in Fig. 2.8 against  $\dot{\epsilon}t$ , together with the equivalent functions for UEF [BSC82a], calculated using similar methods. As we have described for the DE-model, care must be taken around  $\Lambda = 1$  which corresponds to  $\dot{\epsilon}t$  around zero. Low order terms of the Taylor expansion in this region were calculated symbolically using Mathematica and found to be,

$$\begin{aligned} (A_{xx} - A_{yy})|_t &= \frac{4}{5}(\dot{\epsilon}t) - \frac{8}{35}(\dot{\epsilon}t)^3 + \frac{6808}{75075}(\dot{\epsilon}t)^5 + \dots \quad (2.77) \\ \left( \frac{B_{xx} - B_{yy}}{\lambda\dot{\epsilon}} \right) \Big|_t &= \frac{4}{15} + \frac{16}{35}(\dot{\epsilon}t)^2 + \frac{352}{1365}(\dot{\epsilon}t)^4 + \frac{531392}{3828825}(\dot{\epsilon}t)^6 + \dots \end{aligned} \quad (2.78)$$

It is seen from this expansion that in the limit as  $\dot{\epsilon} \rightarrow 0$  that  $(A_{xx} - A_{yy})|_t$  approaches zero, while  $(B_{xx} - B_{yy})/\lambda\dot{\epsilon}|_t$  approaches  $\frac{4}{15}$ .

The steady-state viscosity is found from (2.74) in the limit as  $t \rightarrow +\infty$ . In this limit the second and fourth integrals in (2.74) becomes zero, leaving,

$$\frac{\bar{\eta}(\dot{\epsilon})}{Nn k_B T \lambda} = \frac{1}{4\lambda\dot{\epsilon}} \int_0^{+\infty} \mu(s)(A_{xx} - A_{yy})|_s ds + \epsilon \int_0^{+\infty} \nu(s) \left( \frac{B_{xx} - B_{yy}}{4\lambda\dot{\epsilon}} \right) \Big|_s ds. \quad (2.79)$$

Combining this with the Taylor expansion above we are able to calculate the retarded motion expansion for this model. This may also be accomplished by using the general retarded motion expansion found for the model in Curtiss and Bird [CB81a]. We obtain,

$$\frac{\bar{\eta}}{nNk_B T \lambda} = \left( \frac{1}{60} + \frac{\epsilon}{90} \right) + \left( \frac{-17}{4410} + \frac{17\epsilon}{11025} \right) \lambda^2 \dot{\epsilon}^2 + \dots \quad (2.80)$$

From this expression the zero strain-rate viscosity is found to be,

$$\bar{\eta}(\dot{\epsilon}) = nNk_B T \lambda \left( \frac{1}{60} + \frac{\epsilon}{90} \right). \quad (2.81)$$

The second term in (2.79) is proportional to the link-tension coefficient. This is the only dependence that the viscosity has on this coefficient. Utilising this, we were able to obtain the viscosity for different values of  $\epsilon$  while calculating the second integral just once.

In Fig. 2.9 we have plotted the steady-state extensional viscosity for different values of the link-tension coefficient. The behaviour of these functions is very similar to those presented for UEF [BSC82b]. For values of  $\epsilon$  above approximately  $\epsilon = 0.5$  the functions increase monotonically with strain-rate. This agrees with the second order coefficient which is positive for values of  $\epsilon$  above  $\epsilon \approx 0.4$ . The plateau value of  $\bar{\eta}(\dot{\epsilon})$  is found from (2.74) to be,

$$\lim_{\lambda\dot{\epsilon} \rightarrow +\infty} \frac{\bar{\eta}(\lambda\dot{\epsilon})}{\bar{\eta}(0)} = \frac{15\epsilon}{6 + 4\epsilon}. \quad (2.82)$$

In Chapter 4 we present results from molecular simulations of linear molecules which we are able to compare qualitatively with the predictions of the Curtiss-Bird model.

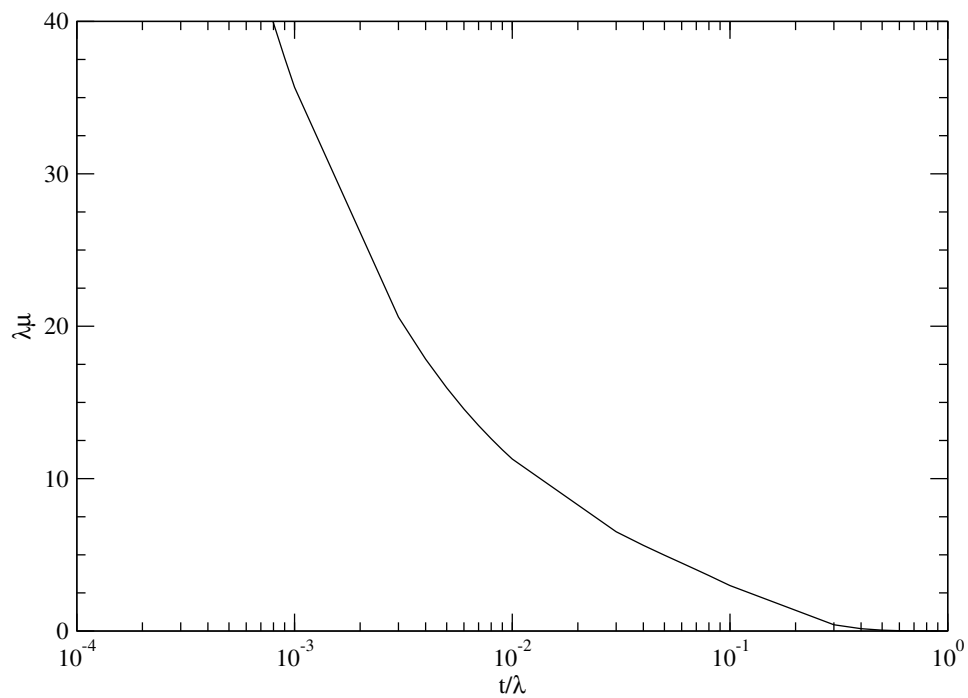


Figure 2.5: The function  $\mu(t)$  using equation (2.73) for  $t/\lambda < 10^{-3}$  and equation (2.71).

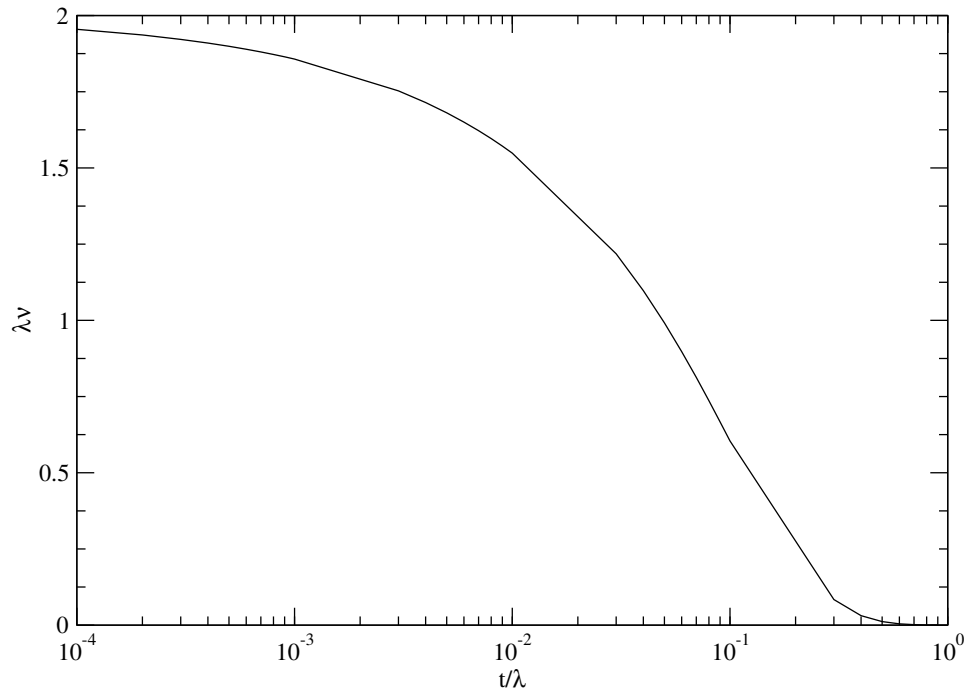


Figure 2.6: The function  $\nu(t)$  is calculated by integrating (2.73)  $t/\lambda < 10^{-3}$  and integrating (2.71) otherwise.

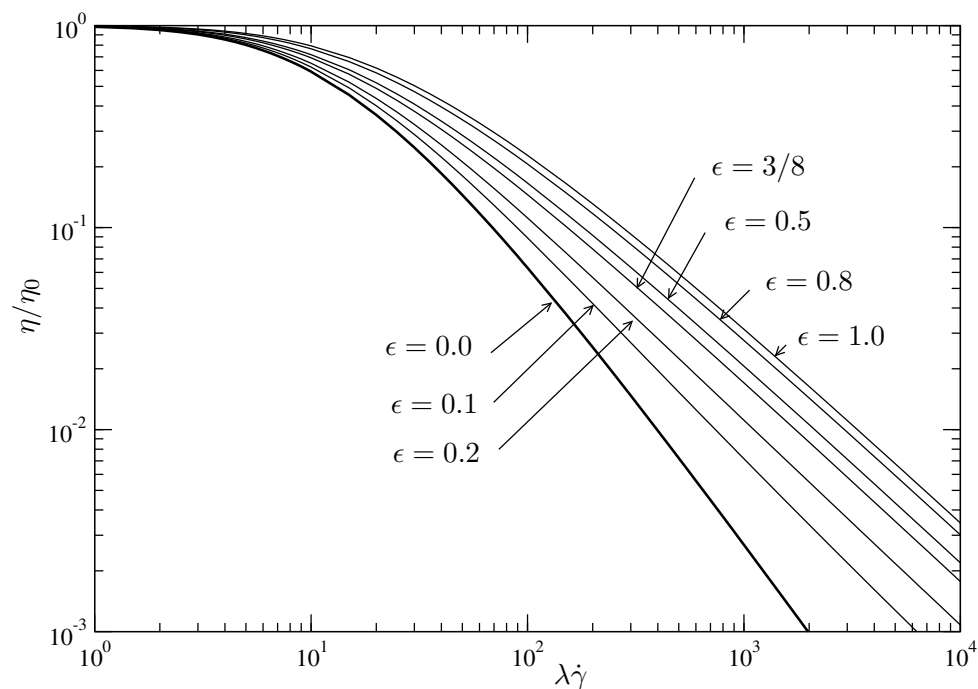


Figure 2.7: Prediction of the Curtiss-Bird model for the steady-state shear viscosity (PCF) as a function of strain rate  $\dot{\gamma}$  and different values of the link tension coefficient  $\epsilon$ . The bold curve  $\epsilon = 0$  corresponds to the prediction of the Doi-Edwards model with the independent alignment approximation. These are our recalculation of results given by Bird *et al.* [BSC82b].

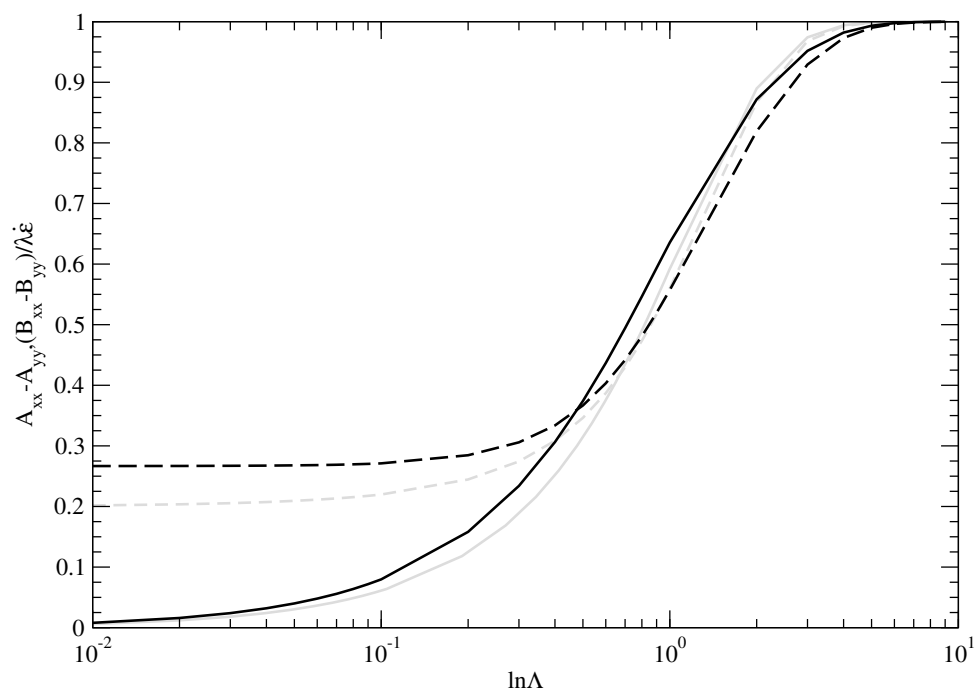


Figure 2.8: Plot of  $A_{xx} - A_{yy}$  (full line) and  $(B_{xx} - B_{yy})/\lambda \dot{\epsilon}$  (dashed line) as a function of  $\ln(\Lambda)$ , for PEF (black line) and UEF (grey line).

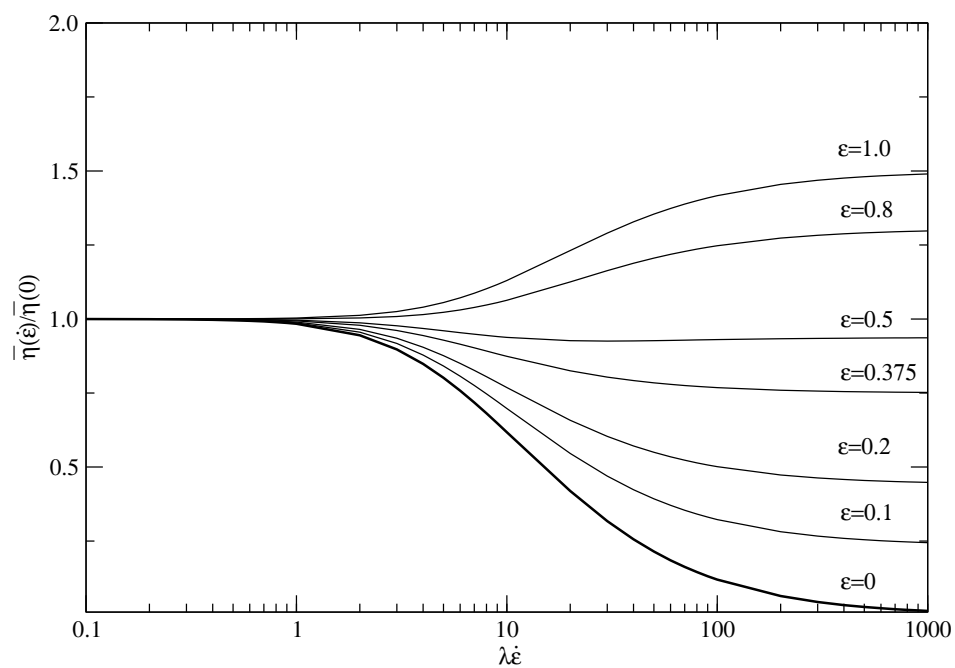


Figure 2.9: Prediction of the Curtiss-Bird model for the steady-state viscosity  $\bar{\eta}/\bar{\eta}_0$  for PEF. This is given as a function of the strain-rate  $\dot{\epsilon}$  and the link tension coefficient  $\epsilon$ . The bold curve  $\epsilon = 0$  corresponds to the prediction of the Doi-Edwards model in the independent alignment approximation.